# Polarized Fluorescence Resonance Energy Transfer Microscopy

Alexa L. Mattheyses,* Adam D. Hoppe,*† and Daniel Axelrod*‡
*Biophysics Research Division, †Department of Microbiology and Immunology, and ‡Department of Physics, University of Michigan, Ann Arbor, Michigan 48109

ABSTRACT Current methods for fluorescence resonance energy transfer (FRET) microscopy of living cells involve taking a series of images with alternating excitation colors in separate camera exposures. Here we present a new FRET method based on polarization that requires only one camera exposure and thereby offers the possibility for better time resolution of dynamic associations among subcellular components. Polarized FRET (p-FRET) uses a simultaneous combination of excitation wavelengths from two orthogonally polarized sources, along with an emission channel tri-image splitter outfitted with appropriate polarizers, to concurrently excite and collect fluorescence from free donors, free acceptors, and FRET pairs. Based upon the throughput in each emission channel as premeasured on pure samples of each of the three species, decoupling of an unknown sample's three polarized fluorescence images can be performed to calculate the pixel-by-pixel concentrations of donor, acceptor, and FRET pairs. The theory of this approach is presented here, and its feasibility is experimentally confirmed by measurements on mixtures of cyan fluorescent protein (CFP), citrine ((Cit) a yellow fluorescent protein variant), and linked fusion proteins (CFP-L16-Cit, CFP-L7-Cit, CFP-L54-Cit) in living cells. The effects of shot noise, acceptor polarization, and FRET efficiency on the statistical accuracy of p-FRET experimental results are investigated by a noise-simulation program.

## INTRODUCTION

Fluorescence resonance energy transfer (FRET) microscopy can be used to visualize the spatial and temporal localization of interactions between labeled proteins within living cells (Kraynov et al., 2000). FRET occurs when an excited donor fluorophore is within the critical transfer distance (~30–100 Å) of an acceptor fluorophore (Lakowicz, 1999). The binding of a donor-labeled protein to an acceptor labeled protein can bring the fluorophores into proximity for FRET, which is thereby used as a qualitative indicator of the binding (Janetopoulos et al., 2001; Oliveria et al., 2003).

In principle, FRET can be detected in a single excitation/emission channel by exciting the sample at the donor excitation wavelength and monitoring a consequent change in acceptor emission. In practice, spatially resolved FRET detection in cells is more complicated, because the local concentrations of free donor, free acceptor, and complexes between the two can all change rapidly and independently. These concentration variations, along with spectral overlap of the donor and acceptor, ''bleed-through'' of donor fluorescence into the acceptor emission channel, and direct acceptor excitation by the donor excitation wavelengths, all combine to render the interpretation of single-channel images ambiguous (Berney and Danuser, 2003).

To surmount these complications, multiple images must be taken with different combinations of excitation and emission filters to allow for the correct separation of FRET from direct emission (Erickson et al., 2001; Gordon et al., 1998; Hoppe et al., 2002; Xia and Liu, 2001). In most cases, these images are obtained with multiple camera exposures because of the need to alternate excitation colors. FRET methods using multiple exposures can be inadequate for visualization of fast molecular, supramolecular, and organelle interactions because some biological processes, such as secretory vesicle fusion with the plasma membrane, occur on a timescale near that of the shortest exposure time of modern charge-coupled device (CCD) cameras or the time required for switching filter channels. A different approach that uses polarization to detect homo-FRET requires only one camera exposure, and is most often used to study protein oligomerization (Gautier et al., 2001) and the organization of membrane proteins (Varma and Mayor, 1998). This technique is useful when detecting energy transfer between two identical fluorophores but it has no ability to track different proteins simultaneously or discriminate between the clustering of one protein or interactions among different proteins.

Here we introduce a new heterotransfer method, polarized FRET (p-FRET), that correctly identifies the presence of FRET based on data gathered from a single exposure. The technique involves the simultaneous direct excitation of both donor and acceptor, each with a different optical polarization. Fluorescence is detected using an emission path image splitter, outfitted with polarizers, that detects the donor fluorescence as well as two polarizations of the acceptor fluorescence. This article presents the qualitative concept, a quantitative theory and image analysis protocol, an analysis of the expected statistical accuracy, and live cell experimental verifications of p-FRET.

*Submitted October 21, 2003, and accepted for publication July 1, 2004.*

Address reprint requests to Alexa L. Mattheyses, Biophysics Research Division, University of Michigan, Ann Arbor, MI 48109. Tel.: 734-647-1828; Fax: 734-764-3323; E-mail: amatthey@umich.edu.



0006-3495/04/10/2787/11 $2.00

doi: 10.1529/biophysj.103.036194

## THEORY

### Qualitative concept

In this work, a ''FRET pair'' is defined as any donor and acceptor pair that are close enough to engage in energy transfer with some nonzero probability (in general less than unity). Otherwise the fluorophores are considered to be free donors and free acceptors that do not participate in energy transfer and only produce direct emission. In a FRET pair, some nonzero fraction of the emission events arise from actual energy transfer. The emission of a FRET pair also contains events in which the donor emits directly and events in which the acceptor is directly excited by the incident light and emits directly. Because of this definition, the probability of transfer does not appear explicitly as a parameter in the theory.

In an experimental system, there are three unknown concentrations, all of which can vary spatially and temporally: free donor ($C_1$), free acceptor ($C_2$), and FRET pair ($C_3$). Therefore, three independent measurements are needed to find a unique solution for all three concentrations. Only two independent measurements can be obtained from any single unpolarized excitation color band, regardless of its particular combination of colors. This is because the acceptor's FRET emission spectrum is indistinguishable from its direct emission spectrum. Therefore, a mixture of the three species in a sample can yield only linear combinations of two emission spectra, that of the donor and the acceptor. In microscope filter sets, the two emission channels are typically optimized around the donor emission and the acceptor emission bands. Any third channel defined by a different emission filter set will only report a linear combination of the donor and acceptor channels and therefore offers no new information. For this reason, a single unpolarized excitation color band is not adequate for measuring FRET.

To make at least three independent measurements in standard FRET, two distinct unpolarized excitation color bands are used alternately in separate camera exposures. Typically, one excitation color band is optimized for donor excitation and the other for acceptor excitation. Switching between two excitation color bands (while observing two emission channels either alternately by filter wheel or simultaneously by image splitter) yields the three measurements from which the FRET contribution can be calculated (Erickson et al., 2001; Hoppe et al., 2002).

The situation can be quite different if the excitation color spectrum is allowed to have a wavelength-dependent polarization, and the polarization-sensitive emission is detected in at least three independent channels. In this case, only one camera exposure is necessary. On the excitation side, this configuration can be achieved experimentally by mixing light from two different sources. To see why this works, consider a simple case in which the excitation consists of simultaneous illumination by two orthogonally polarized bands of different colors, one optimized for donor excitation and polarized N-S in the field of view, and the other optimized for acceptor excitation and polarized E-W. Because the donor's excitation is polarized N-S, then any direct donor emission will tend to maintain this N-S polarization (albeit with some depolarization due to tumbling and nonzero angle between absorption and emission dipoles) (Lakowicz, 1999). In this way the donor emission is ''imprinted'' with the N-S polarization of its excitation. Likewise, any direct acceptor emission will be imprinted with an E-W polarization. Because FRET emission originates with an excited N-S polarized donor, the acceptor FRET emission will tend to maintain this donor-like N-S polarization (if it is not completely depolarized due to FRET). The acceptor's emission is thereby imprinted with polarization information about the source of its excitation, either E-W from direct acceptor emission or N-S from FRET. In principle, the FRET and direct acceptor emission polarizations can have any values (including the case where one or the other is completely depolarized), provided they are not both completely depolarized. With simultaneous orthogonally polarized excitation of both donor and acceptor, the required three images are produced by three emission channels, each with a unique spectrum/polarization combination (p-FRET). In the case discussed above, emission channel 1 can be set as the donor emission wavelength band with no polarization. Channel 2 is the acceptor emission wavelength band with an E-W polarizer. Channel 3 is the acceptor emission wavelength band with an N-S polarizer. All three channels can be imaged simultaneously with an appropriately designed image splitter.

Due to bleed-through, spectral overlap, and partial depolarization, each channel does not represent a single species. However, p-FRET requires that the ratio of intensities observed through each of the three channels ($I_1$:$I_2$:$I_3$) be unique for each of the three types of ''pure'' species (free donor, free acceptor, and FRET pair); i.e., any of the three sets of ratios cannot be linear combinations of the other two. If these ratios are predetermined experimentally in three specially prepared samples containing only a pure species, then the concentrations of donor, acceptor, and FRET present in any unknown sample can be calculated based on the three intensities it produces. Therefore two orthogonally polarized but simultaneous excitation bands and three independent polarization-sensitive emission channels viewed simultaneously with an image splitter can provide all the information needed to calculate the concentrations of free donor, free acceptor, and FRET pairs in a single camera exposure.

Although all of the necessary information is contained in the single exposure, two important practical questions are raised: to what quantitative degree does the acceptor emission have to be polarized for p-FRET to provide useful results? And what happens if the FRET in the

sample is different than the FRET that was premeasured? Both of these questions are addressed here theoretically or experimentally.

## Quantitative theory

Before analyzing images of a sample containing unknown mixtures of the three species, the $I_1$:$I_2$:$I_3$ ratios must be determined separately on three pure samples of cells containing only free donor, only free acceptor, or only linked donor-acceptor FRET pairs. The spectral properties of a FRET pair are thus defined by the particular ratios of the pure FRET sample.

Let $C_j$ represent the concentration of each species $j$ (1 = free donor; 2 = free acceptor; 3 = FRET pair) in an unknown sample, as imaged at a particular pixel. Let $I_i$ represent the fluorescence intensity recorded through channel $i$ at that pixel. Then

$$I_i = \sum_j \alpha_{ij} C_j, \tag{1}$$

where $\alpha_{ij}$ is the fluorescence intensity (in photons/s) observed at a pixel through channel $i$ from a ''pure'' sample $j$ of unit concentration. The $\alpha$ values are determined at each pixel by the specific type of donor and acceptor fluorophores, and also by the features of the particular optical setup used: the alignment, filters, objective, and consequent (possibly spatially dependent) excitation intensities from the two lamp sources. Although the scaling and units of $\alpha_{ij}$ define the meaning of a unit of concentration in the sample, it is the ratios among the $\alpha_{ij}$ that are the most important feature. Given experimental results for $I_i$ on the unknown sample and the set of nine $\alpha_{ij}$ preobtained from the pure samples, one can compute $C_j$ for each pixel in an unknown sample image by Cramer's rule:

$$C_1 = \begin{vmatrix} I_1 & \alpha_{12} & \alpha_{13} \\ I_2 & \alpha_{22} & \alpha_{23} \\ I_3 & \alpha_{32} & \alpha_{33} \end{vmatrix} \Big/ \det \boldsymbol{\alpha},$$

$$C_2 = \begin{vmatrix} \alpha_{11} & I_1 & \alpha_{13} \\ \alpha_{21} & I_2 & \alpha_{23} \\ \alpha_{31} & I_3 & \alpha_{33} \end{vmatrix} \Big/ \det \boldsymbol{\alpha}, \tag{2}$$

$$C_3 = \begin{vmatrix} \alpha_{11} & \alpha_{12} & I_1 \\ \alpha_{21} & \alpha_{22} & I_2 \\ \alpha_{31} & \alpha_{32} & I_3 \end{vmatrix} \Big/ \det \boldsymbol{\alpha},$$

where det $\boldsymbol{\alpha}$ is the determinant of the matrix of $\alpha_{ij}$ parameters.

''Concentration'' here is proportional to the total amount of fluorophore integrated over the optical volume monitored by a single pixel with a weighting derivable from the three-dimensional point spread function. (The numerical value of concentration returned by the procedure refers to the concentration of a deep layer of free fluorophore solution that would produce the same fluorescence as seen at that pixel as described in Materials and Methods.) As such, the calculated concentration generally increases (and then plateaus) with increasing cell thickness. Thus, it is convenient to introduce a normalized concentration $\hat{C}$ that is insensitive to cell thickness:

$$\hat{C}_j = \frac{C_j}{\sum_j C_j}. \tag{3}$$

# MATERIALS AND METHODS

## Optical configuration

An inverted fluorescence microscope (Eclipse TE2000-U, Nikon, Melville, NY) was modified by the addition of a second mercury arc lamp attachment arm to the back of the standard arm (see Fig. 1 *A*). The filters for the first arc

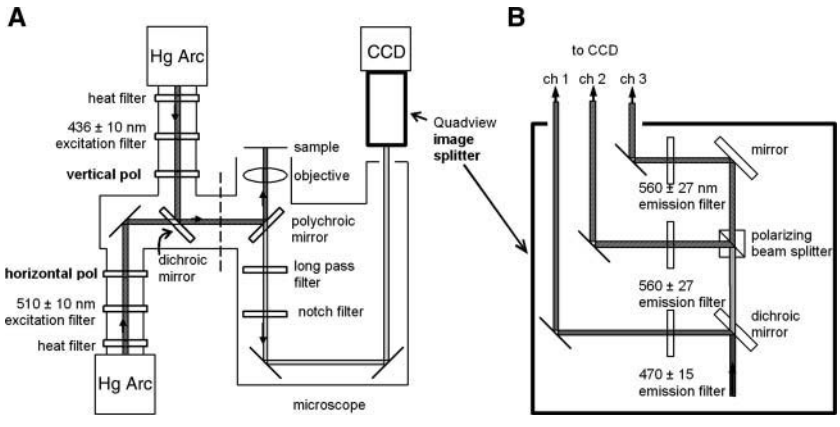


FIGURE 1 Dual mercury arc microscope for p-FRET. (*A*) Schematic overview of the setup. After passing through independent sets of excitation filters optimized for donor and acceptor excitation and through orthogonal polarizers, the beams from the two separate arc lamps are combined with a dichroic mirror. This combined beam is reflected by a polychroic mirror and illuminates the sample. The resulting fluorescence is collected and passed through the polychroic mirror. The emission then passes through the custom Optical Insights QuadView image splitter and focuses as three images on the CCD camera, separated according to wavelength and polarization. Note that the plane of the figure is rotated 90° between the mercury arc section and the microscope section at the plane indicated by the dashed line. The mercury arcs are both in the same horizontal plane (i.e., a top view is shown), whereas the microscope plane is vertical (i.e., a side view is shown). (*B*) Functional schematic view of the inside of the QuadView image splitter.

lamp are a heat absorption filter, a 436 ± 10-nm excitation filter (optimized for cyan fluorescent protein (CFP)), and a vertically oriented film polarizer. The filters for the second arc lamp are a heat absorption filter, a 510 ± 10-nm excitation filter (optimized for citrine (Cit), a variant of yellow fluorescent protein (YFP); Griesbeck et al., 2001), and a horizontally oriented film polarizer. The two excitation color/polarization combinations, each from its separate light source, merge into one light path with a dichroic mirror.

Fluorescence from the sample is collected by a 40× 0.75-N.A. air-immersion objective and then passes through a polychroic 442/514 mirror that allows CFP and Cit fluorescence emission to pass though while reflecting both excitation bands. The emission light passes though a 455 long-pass filter and a 514RB notch filter to further block the excitation light.

The single image of the fluorescence emission from the sample is focused at the entrance to a custom-built Quadview image splitter (Optical Insights, Santa Fe, NM) that creates three separate emission channels. Inside the Quadview, the light is split with a dichroic mirror 505DCXR. (Fig. 1 *B*). The light reflected by this dichroic mirror (wavelengths <505 nm) then passes through a 470 ± 15 nm emission filter; this constitutes ''channel 1''. Channel 1 has no polarization-selecting elements (apart from the slight polarization induced by the dichroic mirror). The light transmitted by the dichroic mirror (wavelengths >505 nm), is split into two separate paths with a polarizing beam splitter. The N-S (''north-south'' as seen through the microscope eyepiece) polarized component passes through a 560 ± 27 nm emission filter; this constitutes ''channel 2''. The E-W (''east-west'') polarized component passes through an identical but separate 560 ± 27 nm emission filter; this constitutes ''channel 3''. Each channel produces a focused image in a distinct quadrant at the CCD camera (Sensicam QE, Cooke, Auburn Hills, MI; 1376 × 1040 pixels, with exposures and data acquisition controlled by the camera's SensiControl software program).

All of the colored and notch filters and dichroic/polychroic mirrors were manufactured by Chroma (Chroma Technology, Rockingham, VT).

## Image processing and analysis

The ''tri-images'', each consisting of three simultaneous views of the sample through the three distinct channels, were collected with exposure times ranging from 0.5 s to 10 s. All of the image processing was performed by custom programs written in Interactive Data Language (IDL, Research Systems, Boulder, CO). First, a background tri-image (a 10-exposure average of a sample consisting only of buffer with the same optical setup as the sample) was subtracted pixel-by-pixel from the sample tri-image. The tri-images were then split into their three separate channel images and aligned with IDL to correct for the shifts and slight relative rotation. After these preparatory steps, every pixel in the scene has an *x*, *y* position and three intensity magnitudes measured in channel 1, channel 2, and channel 3.

To disentangle the contribution of each of the three species to each of the three channels in an experimental sample that contains an unknown mix of the three species, we must first determine $\alpha_{ij}$, the fluorescence intensity of each of the species *i* (at a standard concentration) as reported through each channel *j* (see Eq. 1). Ideally, we would like to measure the $\alpha_{ij}$ values on calibration samples of fluorophores of pure samples with two requirements: a), at known concentrations and pathlength; and b), within a cellular environment. Unfortunately, no sample satisfies both requirements simultaneously. Therefore, the $\alpha_{ij}$ values are separated into a product of two factors such that $\alpha_{ij} = \alpha'_{ij}\beta_j$: a), the throughput $\alpha'_{ij}$ of particular pure species *i* into each of the three channels *j*, with the brightest channel given an arbitrary $\alpha'$ value of unity; and b), a scaling factor $\beta_j$ of this brightest channel representing the photon count observed from a standard solution concentration of species *j*.

Factor $\beta_j$ is measured on pure 1-$\mu$M solutions of CFP, Cit, and CFP-L16-Cit prepared by the methods of Hoppe et al. (2002) and each placed in a coverslip sandwich chamber of 2-mm thickness. These samples were imaged with the microscope setup used for data collection to determine the response of each species. For each of the three pure solution samples, a group of pixels nearest the center of the field of view was used to determine the average intensity per pixel (in CCD counts) of the brightest of the three tri-images.

Factors $\alpha'_{ij}$ can be determined from measurements on living cells that express CFP only, Cit only, and the linked FRET molecule (CFP-L16-Cit) only. Determining the $\alpha$ values with labeled cells (rather than pure and uniform solutions of the three fluorophores) has the advantage that it measures the contribution to each of the three channels of pure fluorophores in their expected cellular environment. Because the relative intensity of the two excitation sources (with their different color bands and polarizations) can vary over the field of view, the $\alpha'_{ij}$ values can also vary over the field of view. This is complicated by the fact that any particular cell does not cover the entire field. Therefore, for each cell type, a series of 10 images was taken with the stage translated laterally so that a large portion of the CCD field of view was covered by part of the cell at least once. Each frame in the series of pictures was background subtracted and aligned as described above, and also threshold discriminated so that only pixels with intensity counts of >200 in at least one channel were considered. Then, a 50 × 50 pixel grid was placed over the image. For every grid box where all the pixels were above the threshold, an average value of the pixels inside the box was computed and assigned to the pixel in the center of the box. Most pixels were well represented by above-threshold values more than once in the set of 10 images, so the average values of pixels in the boxes were also averaged over all the relevant images.

The average value for each of the three channels was then divided by the average value of the brightest of the three channels. These normalized average values at the grid centers were interpolated to all points between grid centers and extrapolated out to the edges where necessary. The resulting image was then smoothed with a 19 × 19 kernal with pixel weights equal to 1. This procedure was repeated for each of the three species, so that every pixel in the field has nine $\alpha'_{ij}$ values assigned. Finally, the $\alpha'_{ij}$ values were multiplied by the appropriate $\beta_j$ to obtain $\alpha_{ij}$ for each pixel.

The final step is to determine the unknown mix of free donor, free acceptor, and FRET concentrations in the experimental sample. For each pixel in an unknown sample there is some intensity count in each channel represented by $I_1$, $I_2$, and $I_3$. Cramer's rule (Eq. 2) is then applied to Eq. 1 to produce a concentration of free donor, free acceptor, and FRET ($C_1$, $C_2$, $C_3$) for every pixel. The result is three spatial maps of the relative concentrations of free donor, free acceptor, and FRET pairs, respectively. In the spatial maps, computed concentrations less than zero were set equal to zero. These spatial maps are then normalized into fractions of total concentration $\hat{C}_1$, $\hat{C}_2$, $\hat{C}_3$ (Eq. 3) to eliminate effects of cell thickness.

## Simulation of noise

To evaluate the effects of shot noise in the raw ''input'' intensities $I_{1\text{-}3}$ on the computed normalized concentrations, an IDL program was written, which simulates the input photon count intensities in each channel by a Poisson-distributed random variable. The mean intensity chosen for each channel is based on a set of appropriate $\alpha_{ij}$ values that depend on the assumed polarizations and FRET efficiency (see below). Then for each selection of input photon counts and input set of normalized concentrations $\hat{C}_{1\text{-}3}$, the program computes an output set of $\hat{C}'_{1\text{-}3}$ by use of Eq. 2. Because of the noise inherent in the Poisson-generated photon counts (i.e., the *I* values are somewhat different for every run of the program), a given output of a normalized concentration (say, $\hat{C}'_3$) can arise from a range of input normalized concentrations $\hat{C}_3$. The resulting standard deviation in input $\hat{C}_3$ is presented as a function of the total input photon counts ($I_1 + I_2 + I_3$), averaged over 5000 runs. The standard deviation in $\hat{C}_3$ also can be a function of $\hat{C}_3$. In the application of this program presented here, $\hat{C}_3$ was varied from 0 to 1 in increments of 0.05, and $\hat{C}_1$ was set equal to $\hat{C}_2$.

To evaluate how large the polarization of the acceptor fluorescence must be to compute meaningful normalized concentrations (i.e., above the noise level), the IDL noise simulation program described above was used in sequential runs with different input and $\alpha_{ij}$ parameters, corresponding to different acceptor emission polarizations. The polarization of Cit was changed for each run such that the relative response of Cit in channel

3/channel 2 (i.e., $\alpha_{32}/\alpha_{22}$) ranged from 0:1 to 1:1 in increments of 0.1. For the sake of concreteness in the calculation, we assumed certain definite (entirely reasonable and clearly not best-case) relationships: when FRET events occurred, they were assumed to completely depolarize the emission; and the $\alpha_{i3}$ values (which specify the fluorescence for species 3, pure FRET-pair molecules) correspond to a 40% FRET efficiency in species 3. A similar approach was used to evaluate the effect of FRET transfer efficiency on the statistical uncertainty p-FRET measurements. The IDL noise simulation program was run sequentially with different input and $\alpha_{ij}$ parameters, corresponding to different transfer efficiencies. Direct Cit emission was assumed to have a channel 3/channel 2 ratio $\alpha_{32}$:$\alpha_{22}$ of 0.7, which corresponds to the experimental situation. As above, pure FRET emission was assumed to be completely depolarized; i.e., far from a ''best case.'' The noise simulation program was run numerous times for each set of acceptor emission polarizations or FRET efficiencies and the resulting standard deviations within each set were computed as described above. For display here, we report only the standard deviations as a function of acceptor emission polarization or FRET efficiency for the situation where the concentrations of all three species are equal ($C_1 = C_2 = C_3$).

To generate the statistical uncertainties shown in Fig. 6, *B* and *C*, a set of $\alpha$ parameters must be chosen to correspond to the contribution from pure donor ($\alpha_{i1}$), pure acceptor ($\alpha_{i2}$), and ''pure FRET'' ($\alpha_{i3}$) for each location on the plots. At all points in both figure panels, $\alpha_{i1}$ was assigned the values (0.50, 0.099, 0.23), which are the actual observed experimental values for CFP. Also at all points in both panels, pure acceptor was assigned the experimental values $\alpha_{12} = 0.00092$ and $\alpha_{22} = 0.70$. For Fig. 6 *C*, which shows the effect of varying transfer efficiency, the remaining pure acceptor value $\alpha_{32}$ was assigned the constant experimentally observed value of 0.49. For Fig. 6 *B*, which shows the effect of varying acceptor polarization (particularly to lower values), $\alpha_{32}$ was varied between 0.0 and 0.70.

The intensities observed from ''pure FRET'' that give rise to the $\alpha_{i3}$ values are actually composites, because a FRET molecule can emit three different ways upon illumination with the simultaneous two-color polarized light of p-FRET: when its donor or acceptor are directly excited (without energy transfer) and also when the acceptor emits because of energy transfer from the donor. Therefore, the $\alpha_{i3}$ values are a linear combination arising from these three modes:

$$\alpha_{i3} = (1 - E)\alpha_{i1} + \alpha_{i2} + E\alpha''_{i3}, \quad (4)$$

where $E$ is the probability that an excitation of the donor gives rise to an excitation of the acceptor (i.e., the transfer efficiency). For Fig. 6 *B*, $E = 0.4$, and for Fig. 6 *C*, $E$ varied from 0.05 to 0.5. Parameters $\alpha''_{i3}$ give the set of three intensities that would be observed from a unit concentration of a hypothetical FRET pair that has a 100% transfer efficiency and contains no contributions at all due to direct excitation/emission of either its donor or its acceptor. As a worst case, we assume that FRET completely depolarizes the emission by setting $\alpha''_{13} = 0.0013$ (equal to that seen with pure Cit), $\alpha''_{23} = 1$, and $\alpha''_{33} = 1$. To compute $\alpha_{i3}$ by Eq. 1, the $\alpha_{i1}$ values are set at (0.50, 0.099, 0.23) as above.

## Cell culture and transfection of COS cells

COS7 cells obtained from American Type Culture Collection (ATCC, Manassas, VA) were grown in Dulbecco's modified Eagle's medium supplemented with 10% fetal bovine serum (Gibco BRL, Gaithersberg, MD) (heat-inactivated at 56°C for 45 min) and 100 unit/mL of penicillin/streptomycin mixture (Sigma, St. Louis, MO) at 37°C with 5% $CO_2$. COS cells were plated on coverglasses 4 h before transfection. Transfection was carried out 24 h before the experiment with 1 $\mu$g total plasmid DNA and 2 $\mu$l FuGene6 (Roche, Basel, Switzerland). During microscopic observation, the cells were maintained at room temperature in Ringer's buffer: 155 mM NaCl, 5 mM KCl, 2 mM $CaCl_2$, 1 mM $MgCl_2$, 2 mM $NaH_2PO_4$, 10 mM HEPES, and 10 mM glucose.

## Generation of fluorescent controls

The plasmids pCFP-N1, pCit-N1, and pCFP-Cit are described in Hoppe et al. (2002). CFP-Cit was used as the ''standard'' FRET molecule and was denoted CFP-L16-Cit because it had a 16 amino acid linker between the donor CFP and the acceptor Cit. Another linked molecule with only seven amino acids between the fluorescent proteins, denoted CFP-L7-Cit here, was generated in an analogous method. Briefly, polymerase chain reaction (PCR) was used to amplify CFP and this was inserted into the pCit-C1 vector between restriction sites *Bsp*EI and *Eco*RI to yield the DNA sequence,

5-Cit-TCC GGA ATC GAA GGC AGA TCT-CFP-3′

with amino acid linker SGIEGRS. A lower FRET-efficiency molecule was generated by increasing the number of amino acids between the fluorescent proteins to 54, denoted Cit-L54-CFP here. The DNA coding for the PBD domain of hPAK1 was amplified by PCR and inserted into Cit-L7-CFP between the *Bsp*EI and *Bgl*II restriction sites to yield the following DNA structure,

5′-Cit-TCC GGA AAA GAG CGG CCA GAG ATT
TCT CTC CCT TCA GAT TTT GAA CAC ACA ATT
CAT GTC GGT TTT GAT GCT GTC ACA GGG GAG TTT
ACG GGA ATG CCA GAG CAG TGG GCC CGC TTG
CTT CAG ACA TCA AAT ATC ACT AAG TCG GAG
CAG AAG GGA AGA TCT – CFP-3′

that codes for 54 amino acids:

SGKERPEISLPSDFEHTIHVGFDAVTGEFTG
MPEQWARLLQTSNITKSEQKGRS.

## Determination of FRET efficiency by fluorescence lifetime

The FRET efficiency of CFP-L7-Cit, CFP-L16-Cit, and CFP-L54-Cit were determined in living COS cells by analyzing the donor fluorescence lifetime as previously described (Hoppe et al., 2002). Briefly, light from a mode-locked, frequency-doubled, and pulse-picked Ti:Sapphire laser (Spectra Physics, Mountain View, CA) (1-ps-wide pulses of 436 nm at 8 MHz) was used to illuminate an ~5-$\mu$m spot. Time-correlated single-photon counting was conducted with a PMT (H3809, Hamamatsu Photonics, Hamamatsu, Japan) and a TimeHarp photon counting card (PicoQuant GmbH, Berin-Adlershof, Germany). CFP decays were analyzed with FluoFit 3.0 (PicoQuant) and used to calculate the FRET efficiencies as described (Hoppe et al., 2002).

# RESULTS

## Tests on transfected cells with CFP-L16-Cit

The p-FRET method was first tested with singly transfected COS cells (either CFP alone (donor), Cit alone (acceptor), or CFP-L16-Cit alone (FRET pair)) to check whether polarized FRET would correctly report the sole presence of each species. A typical set (chosen from a total of over 50 sets) of

raw images from these cells is shown in Fig. 2. The corresponding nonnormalized and normalized concentrations of donor, acceptor, and FRET, as computed according to the procedure described in Methods, are displayed in pseudocolor in Fig. 3. As expected, the nonnormalized images show a higher concentration (as integrated over the depth of the cell) near the nucleus where the cell is thicker; this effect disappears upon normalization. In each case, the only type of fluorophore found by p-FRET in significant quantity is the fluorophore type that is known to be present. In particular, there is never a significant amount of FRET seen in the pure CFP or pure Cit cells. These experiments show that the technique correctly detects each species when it is present in isolation.

The method was tested next on three combinations of doubly transfected COS cells (CFP and Cit; CFP-L16-Cit and CFP; CFP-L16-Cit and Cit) and also on triply transfected COS cells (CFP-L16-Cit, CFP, and Cit). Nonnormalized and normalized computed concentrations of the three species are displayed in pseudocolor in Fig. 4. Within groups of cells transfected with multiple plasmids (e.g., CFP and CFP-L16-Cit), the individual cells expressed different absolute amounts of each species, and therefore the ratios varied from cell to cell. The normalized concentrations are uniform within a cell. As expected, only cells transfected in part with CFP-L16-Cit show any amount of FRET. Cells expressing CFP-L16-Cit and CFP do not show any Cit (Fig. 4 *B*), and cells expressing CFP-L16-Cit and Cit do not show any CFP (Fig. 4 *C*). Cells transfected for all three species (CFP, Cit, and CFP-L16-Cit) show varying amounts of all species in different cells (Fig. 4 *D*).

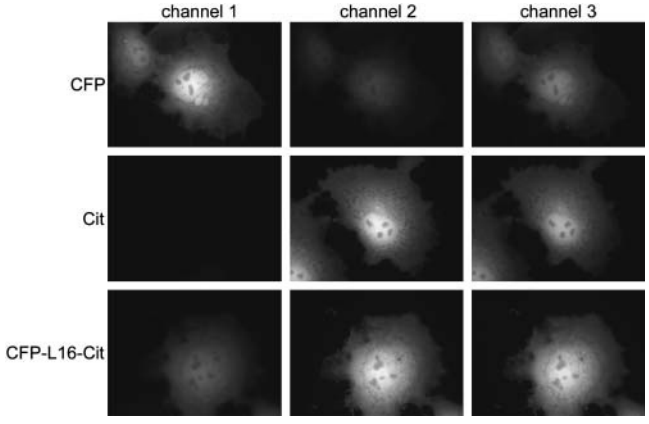


FIGURE 2 P-FRET images (raw data, after background subtraction) of COS cells expressing either CFP alone, Cit alone, or CFP-L16-Cit alone, as observed in channels 1, 2, and 3. The varying intensities in each channel indicate the response of each fluorophore to the excitation as seen through the particular emission filters. The p-FRET technique requires that the response of the linked molecule is not a linear combination of the responses of pure donor and pure acceptor. The grayscale ranges always start from zero photon counts but reach different maxima for the three different rows. The maxima are: 6948 (CFP); 5888 (Cit); and 11036 (CFP-L16-Cit).

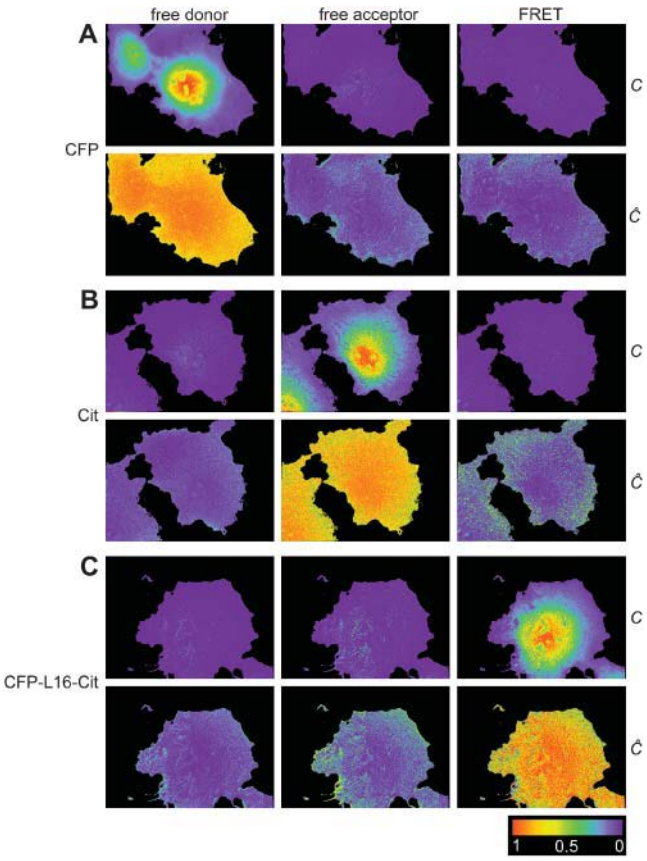


FIGURE 3 Processed p-FRET images of the COS cells shown in Fig. 2 expressing either CFP alone (*A*), Cit alone (*B*), or CFP-L16-Cit alone (*C*). The columns show the concentrations of donor, acceptor, and FRET as indicated. In each group of two rows, the top row is the nonnormalized concentration $C$ (scaled for the display so that the brightest pixel is set equal to 1 on the color bar) and the bottom row is the corresponding normalized concentration $\hat{C}$. The color scales of the nonnormalized $C$ panels always start from deep purple for zero concentration but reach different maxima (*red*) for the three different rows. The maxima (in equivalent $\mu$M) are: 0.84 (CFP); 0.69 (Cit); 0.76(CFP-L16-Cit). The color bar for the normalized concentrations is the same for all three species and is shown in the lower right.

## Tests with other FRET pairs

In the above tests, the FRET pair incorporated in the cells (CFP-L16-Cit) was known to be the same as used for obtaining the calibration $\boldsymbol{\alpha}$ matrix values. However, the robustness of the p-FRET method should also be tested in a more realistic situation that models biologically relevant but unknown FRET molecules that might be different from the known FRET standard used for setting up $\boldsymbol{\alpha}$. Therefore, the method was tested on two groups of unknown samples with different FRET molecules than present in the FRET calibration sample (which remained CFP-L16-Cit as before).

The efficiency of the FRET molecules was measured by fluorescence lifetime. The efficiency of CFP-L16-Cit is 35 $\pm$ 0.63%, the efficiency of CFP-L7-Cit is 36.3 $\pm$ 0.60%, and the efficiency of CFP-L54-Cit is 27.7 $\pm$ 0.58%. Where the error is calculated as the standard error of the mean for data

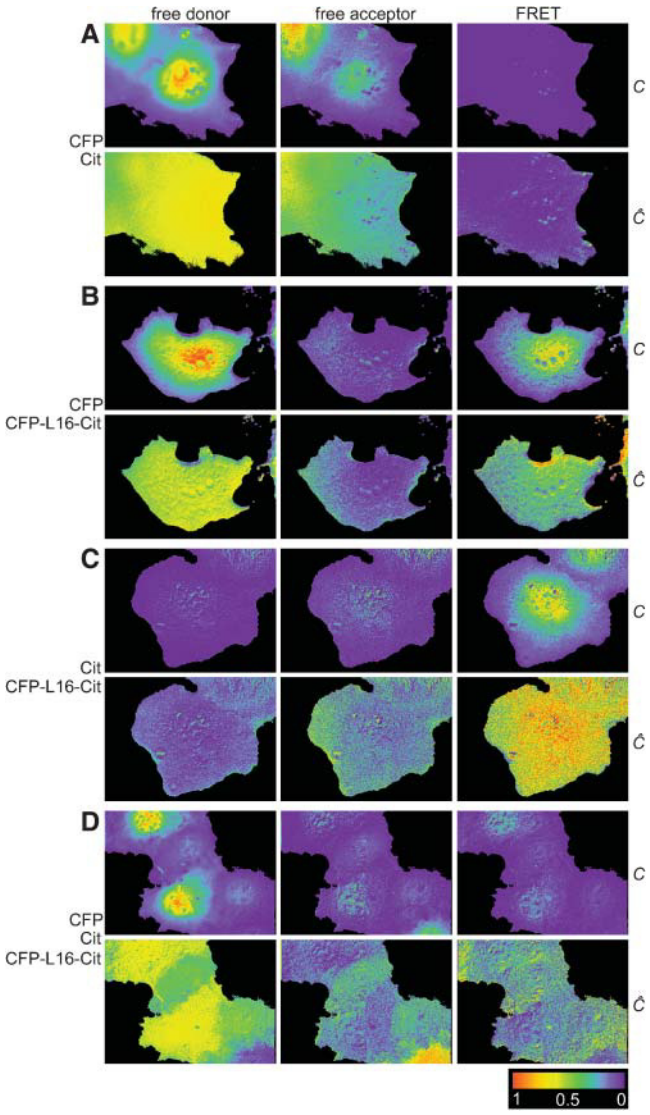


FIGURE 4 Processed p-FRET images of COS cells coexpressing combinations of multiple transfections of CFP and Cit (*A*), CFP and CFP-L16-Cit (*B*), Cit and CFP-L16-Cit (*C*), and CFP, Cit, and CFP-L16-Cit (*D*). For each combination, two rows of images are presented. In each group of two rows, the top row is the nonnormalized concentration $C$ (scaled for the display so that the brightest pixel is set equal to 1 on the color bar) and the bottom row is the corresponding normalized concentration $\hat{C}$. The color scales of the nonnormalized $C$ panels always start from deep purple for zero concentration but reach different maxima (*red*) for the three different rows. The maxima (in equivalent $\mu$M) are: 1.19 (CFP and Cit); 0.27 (CFP and CFP-L16-Cit); 0.45 (Cit and FRET); 0.96 (CFP, Cit, and CFP-L16-Cit). The color bar for the normalized concentrations is the same for all three species and is shown in the lower right.

collected from five cells expressing each molecule independently.

COS cells in one group were transfected with CFP-L7-Cit, a FRET pair with approximately equally efficient energy transfer as compared to the standard CFP-L16-Cit but with a different structure; COS cells in the other group were transfected with CFP-L54-Cit, a FRET pair with less efficient energy transfer than the standard CFP-L16-Cit. In each group, transfections were either ''singles'' (FRET pair only); two types of ''doubles'' (FRET pair + CFP and FRET pair + Cit); and ''triples'' (FRET pair + CFP + Cit). In each group, cells with the single transfections appear exclusively as FRET in the computed concentrations (Fig. 5, *A* and *D*). Cells with double transfections show varying ratios of the species included in the cotransfection but never the species missing from the cotransfection (Fig. 5, *B*, *C*, *E*, and *F*). Cells cotransfected with all three species showed varying amounts of all species in different cells (not shown).

These results demonstrate that the computed images based on the p-FRET method are qualitatively accurate in living cells, with no ''false positives'' for FRET or for isolated donor and acceptor out of the >50 cells evaluated for each cell type. The technique is robust in the sense that this qualitative accuracy does not depend upon the ''standard''

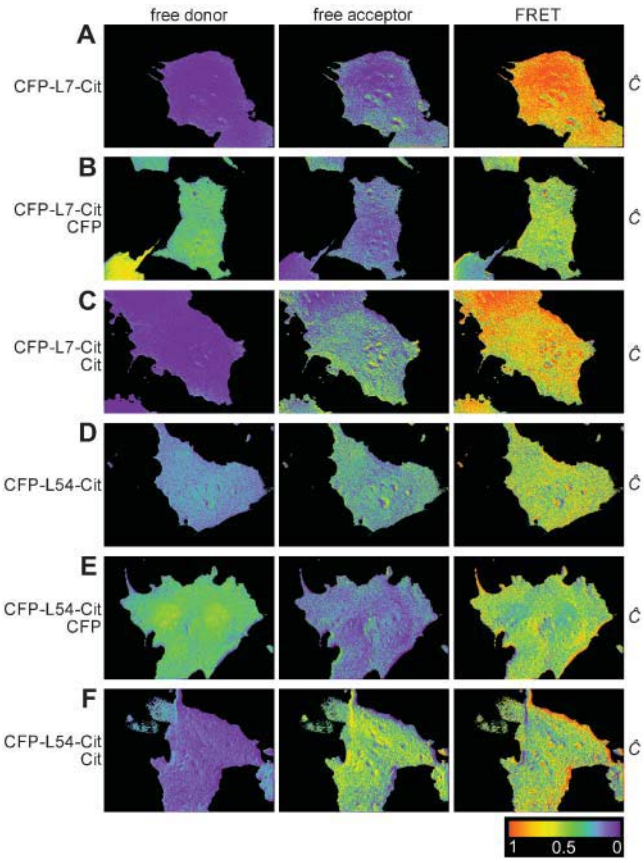


FIGURE 5 Normalized p-FRET images of COS cells in the case where the FRET pair in the cells is different from the FRET pair used for calibration. The $\alpha_{ij}$ were obtained from a ''standard'' sample of CFP-L16-Cit for all the calculations. Cells depicted in panels *A–C* contain FRET pairs that are approximately equally efficient to the standard. (*A*) Single transfection with CFP-L7-Cit. (*B*) Double transfection with CFP-L7-Cit and CFP. (*C*) Double transfection with CFP-L7-Cit and Cit. Cells depicted in panels *D–F* contain FRET pairs that are less efficient than the standard. (*D*) Single transfection with CFP-L54-Cit. (*E*) Double transfection with CFP-L54-Cit and CFP. (*F*) Double transfection with CFP-L54-Cit and Cit.

FRET molecule being the same as the (generally unknown) FRET pair that might occur in a cellular sample.

### Statistical accuracy of p-FRET: number of required photons

An IDL program, developed to investigate the effects of shot noise on the accuracy of computed normalized concentrations of p-FRET (see Materials and Methods), was used to predict the expected uncertainty (i.e., standard deviation) in the calculated estimate for normalized FRET concentration $\hat{C}_3$. As expected, this uncertainty in $\hat{C}_3$ is a strong function of the total number of recorded photons and also a weak function of all three concentrations $\hat{C}_1$, $\hat{C}_2$, and $\hat{C}_3$. The IDL program calculates the uncertainty in $\hat{C}_3$ as a function of the calculated estimate for $\hat{C}_3$, in the particular case that $\hat{C}_1 = \hat{C}_2$. The result, shown in Fig. 6 *A*, depicts the total number of input photons from all channels (on the ordinate axis) that are required to produce less than a particular standard deviation in $\hat{C}_3$ for a given calculated $\hat{C}_3$ (on the abscissa axis).

The recorded number of photons (as observed in any pixel) is expressed as the sum of photon counts in the three raw images. (The photon count is the CCD camera count multiplied by the camera's A/D conversion factor in electrons/count). As expected, a higher number of photons provides a lower uncertainty in $\hat{C}_3$, and the absolute uncertainty increases slowly with increasing $\hat{C}_3$.

The key question is: where do typical results from cell images reside on this graph? For our particular experiments on cells containing a mixture of all three species (shown in Fig. 4 *D*), the gray cross symbols in Fig. 6 *A* indicate a random selection of on-cell pixels, each plotted according to its total photon count and calculated $\hat{C}_3$. The brightest (usually most central) parts of the cells (the upper end of the region populated by *gray crosses* in Fig. 6 *A*) have an uncertainty in $\hat{C}_3$ of $\sim\pm0.1$, and the dimmest (usually peripheral) parts have an uncertainty in $\hat{C}_3$ of $\sim\pm0.3$.

### Statistical accuracy of p-FRET: polarization requirement

The same program used for noise analysis was modified to investigate the effect of acceptor emission polarization on the standard deviation of the computed normalized FRET concentrations $\hat{C}_3$. The program was run 10 times, each time with a different input ratio of acceptor polarization ratio $\alpha_{32}$:$\alpha_{22}$ (see Materials and Methods). As described above, the program calculated the uncertainty in $\hat{C}_3$ as a function of the calculated estimate for $\hat{C}_3$ for each input ratio of acceptor signal. The case where $\hat{C}_1 = \hat{C}_2 = \hat{C}_3 = 1/3$ was selected for each ratio. The result, shown in Fig. 6 *B*, depicts the minimum number of input photons (as described above) needed to produce less than a certain standard deviation in $\hat{C}_3$ (around its mean of 1/3) for varying polarization ratios (on the abscissa axis). The minimum number of photons needed to give a particular standard deviation is less if the acceptor is more polarized and more if the acceptor is less polarized, as would be expected. As the ratio of acceptor polarization approaches unity (i.e., unpolarized), the number of photons needed for the technique approaches infinity, also as expected. The gray line indicates where Cit, the acceptor in the experiments described, lies on this chart.

### Statistical accuracy of p-FRET: FRET efficiency

The program used for noise analysis was further modified to investigate the effect of FRET efficiency on the standard deviation of the computed normalized FRET concentrations $\hat{C}_3$. The program was run 11 times, each time with a different FRET efficiency (see Materials and Methods). As described above, the program calculated the uncertainty in $\hat{C}_3$ as a function of the calculated estimate for $\hat{C}_3$ for each input FRET efficiency. The case where $\hat{C}_1 = \hat{C}_2 = \hat{C}_3 = 1/3$ was selected for each efficiency. The result, shown in Fig. 6 *C*, depicts the minimum number of input photons (as described above) needed to produce less than a certain standard deviation in $\hat{C}_3$ (around its mean of 1/3) for the FRET efficiency specified by the position along the abscissa axis. The minimum number of photons needed to give a particular standard deviation is less for higher transfer efficiencies and more for lower transfer efficiencies as would be expected.

## DISCUSSION

We have presented a new technique for obtaining FRET measurements in living cells. Polarized FRET uses excitation light with wavelength dependent polarization to imprint a record of the excitation mode (direct or FRET) upon the fluorescence emission. After premeasuring the throughput of the system for the polarized fluorescence of pure donor, pure acceptor, and pure FRET pairs, the relative concentrations of free donor, free acceptor, and FRET pairs can be determined inside living cells. This technique is unique because polarization imprinting allows the simultaneous collection of all the data necessary to calculate the concentrations of the three species in a single camera exposure.

The p-FRET technique was applied to living cells and was shown to yield qualitatively reliable results. The fluorophores CFP and Cit (a YFP variant) are popular for investigating intracellular associations by FRET and proved to be suitable for the p-FRET technique. The technique in theory requires only that the acceptor emission from direct excitation and from FRET are not both completely depolarized. Complete depolarization could occur, for example, if the acceptor absorption and emission dipoles were far from parallel, or if the acceptor tumbled extensively during its excited state lifetime. The question of what minimum acceptor emission polarization is required in practice to yield reliable results for normalized FRET-pair concentration is a question of signal/noise. Therefore, the effect of

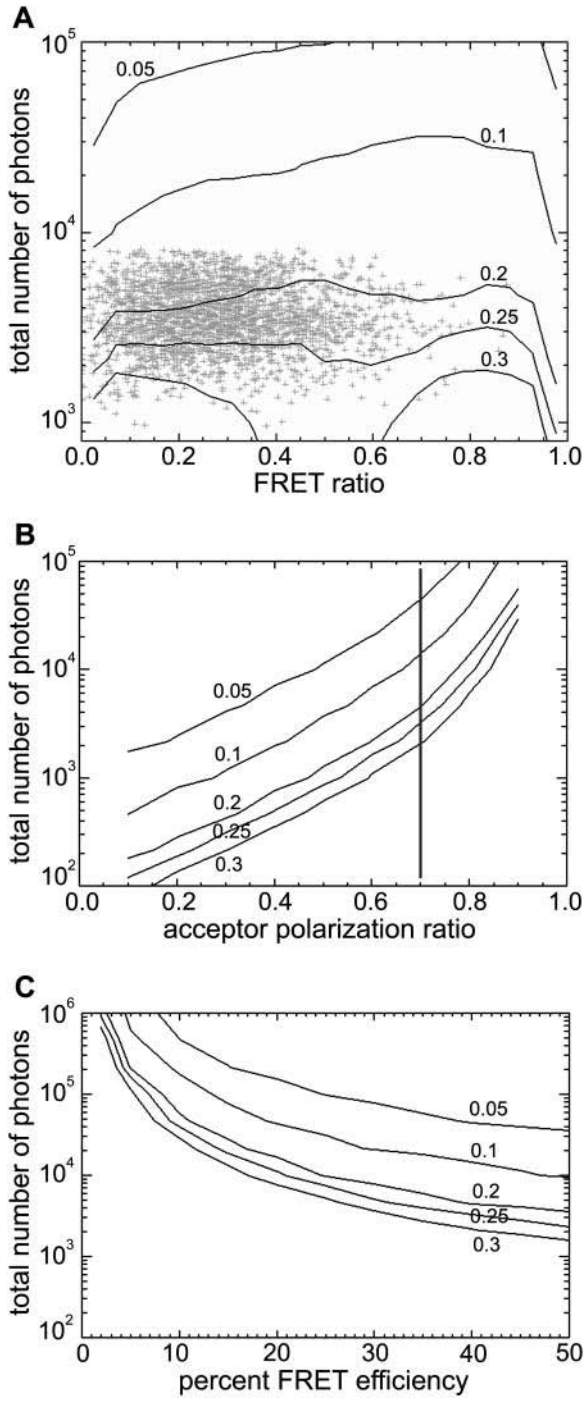


FIGURE 6 (*A*) The effect of shot noise on statistical accuracy of the computed results. Shown here is the total number of photons $I_1 + I_2 + I_3$ that need to be collected per pixel, versus the normalized FRET concentration $\hat{C}_3$, for various target standard deviations in $\hat{C}_3$. To generate this figure, $\hat{C}_1 = \hat{C}_2$ was assumed; other relative concentrations of pure donor and acceptor would generate similar but quantitatively different graphs. The gray-cross data points represent pixels randomly selected from an on-cell region of the second cell from the top in Fig. 4 *D*. (*B*) The effect of acceptor polarization on the statistical accuracy of the computed results. Shown here is the total number of photons $I_1 + I_2 + I_3$ that need to be collected per pixel, versus the acceptor polarization ratio ($\alpha_{32}$:$\alpha_{22}$), for various target standard deviations in $\hat{C}_3$. $\hat{C}_1 = \hat{C}_2 = \hat{C}_3 = 1/3$ is assumed. The gray line is the polarization ratio of Cit in the experiments reported here. (*C*) The effect of FRET transfer efficiency on the statistical accuracy of the computed results. Shown here is the total number of photons $I_1 + I_2 + I_3$ that need to be collected per pixel, versus FRET efficiency for various target standard deviations in $\hat{C}_3$. $\hat{C}_1 = \hat{C}_2 = \hat{C}_3 = 1/3$ is assumed.

different acceptor emission polarizations was investigated with a noise simulation program. As expected, when the acceptor emission is more polarized, the number of photons needed to obtain a certain level of accuracy is less than when the acceptor emission is less polarized. The number of photons needed approaches infinity when the acceptor is completely depolarized (Fig. 6 *B*). This limit is expected because a completely depolarized direct acceptor emission is indistinguishable from a completely depolarized FRET emission in the p-FRET technique. In the experiments here, the acceptor's (Cit) polarization ratio (defined as channel 3/channel 2 intensity) was 0.7, which is sufficiently polarized to yield useful results.

Several factors contribute to the polarization ratio as observed in a p-FRET experiment. The first is the intrinsic polarization of the isolated acceptor emission, which may be a function of its environment and the particular excitation and emission wavelengths used. Secondly, spectral overlap (which can lead to acceptor excitation by the donor excitation color as well as the acceptor excitation color, the two of which are polarized orthogonally), can cause an apparent depolarization as evidenced in the channel 3/channel 2 ratio. Thirdly, high-aperture objectives lead to depolarization (Axelrod, 1979). Nonetheless, the polarization requirement should not seriously limit the choices of fluorophore pairs. Because p-FRET works with the CFP/Cit pair, it is also likely to work with other FRET pairs in the fluorescent protein family. The polarization ratio for any potential acceptor can be measured and judged with Fig. 6 *B* to see how well it will perform.

P-FRET was shown to be qualitatively reliable even if the experimental sample contained a different FRET pair than the one used for calibration. This shows the robustness of the technique for use on biological systems in which the FRET-pair efficiency is not known and may be different from that of the calibration sample. The quantitative computed concentrations are most likely inaccurate in this case. Nonetheless, the technique does not falsely report the presence of FRET or free donor or free acceptor where it does not exist, so it is useful as a qualitative indicator of FRET and free donors or acceptors.

All of the measurements shown were performed experimentally on FRET samples with relatively low FRET efficiencies (<37%). These efficiencies are reasonably typical and in the middle of the range observed by others for mutants of CFP and YFP (e.g., 15–47% depending on the conformation of a particular linker protein as observed by Habuchi et al., 2002). The accuracy of p-FRET for various FRET efficiencies also was investigated theoretically. The

results showed that low-efficiency FRET can be detected with p-FRET given a large enough (but still reasonable) number of photons. For example, the relative concentration of FRET molecules with an efficiency of 5% can be detected by p-FRET with mean SD $\pm 0.1$ if $10^6$ photons are collected. This is a feasible number of photons to collect with our system, and straightforward ways to further improve photon collection are discussed below.

An essential feature of polarized FRET is its potential for viewing fast interactions. The minimum time resolution is limited by two factors: a), the CCD camera's shortest interexposure readout time; and b), the exposure time that is set by the finite number of detected photons in any pixel of interest, which gives rise to shot noise. The effect of shot noise on p-FRET was investigated here with a theoretical program that inputs a certain set of ''observed'' mean intensities corresponding to a certain mix of input concentrations among the three species but with the actual count provided from a Poisson-distributed random number generation. The program then recovers an estimate of the input concentrations, using the same mathematical procedure used to derive concentrations at each pixel in experimental images. Not surprisingly, the simulated shot noise causes the recovered value to deviate randomly from the input values. However, a surprisingly small number of photons can give a fairly reasonable agreement between input and output concentration. For example, only 4000 total photons can provide measurement of normalized FRET concentration $\hat{C}_3$ to a precision of $\pm 0.2$. This is a typical number of photons seen with exposures of 0.5–10 s (depending on sample brightness).

Our experiments were intended only to demonstrate the feasibility of the technique, and did not employ easily implemented approaches to maximize the number of detected photons. Using a CCD camera with a higher quantum efficiency (such as a ''back-thinned array'') and using the microscope's base port (instead of the trinocular head port as done here) would substantially increase the photon throughput. A higher aperture objective can excite the sample with more intense light and gather significantly more emitted photons. However, very large apertures can lead to depolarization (Axelrod, 1979), which will reduce the advantage of higher photon rates. Binning could also be employed to increase the number of photons while sacrificing lateral resolution. On the other hand, an image intensifier or electron-multiplying CCD would not assist in overcoming shot noise but only in overcoming readout noise, which we did not consider in our noise estimates.

An important benefit of p-FRET is that all the information can be collected in a single exposure. Even if a biological event that presents a FRET signal is shorter than the exposure time, all the necessary information is still captured in that one exposure (albeit with decremented signal/noise). In standard FRET, at least two sequential exposures with different excitation colors are necessary to distinguish a FRET event. To detect transient events in standard FRET, very rapid synchronized chopping can be arranged, but the extra time needed for the additional CCD readouts plus the dead time during color switching, limits the overall time resolution.

The ratio of intensities in the two orthogonally polarized excitation beams strongly affects the $\alpha$ values that are used in the calculations for the concentration of each of the three species. With incoherent arc lamp epi-illumination as used here, the ratio is fairly uniform over the field of view (although we still compute $\boldsymbol{\alpha}$ as a spatially varying matrix of values based on reference images of singly labeled cells). However, with coherent laser epi-illumination, a different interference fringe pattern for each color makes the intensity ratio highly dependent on both lateral ($x$-$y$)-position and also upon focal plane $z$-position. This $z$-dependence invalidates determination of the $\boldsymbol{\alpha}$ matrix measured from any reference sample for which refocusing from the experimental sample is required. With laser-based total internal reflection (TIR) illumination, this $z$-dependence problem is completely avoided, because the evanescent field, including its interference fringes, are essentially two-dimensional relative to the microscope's depth of focus. Therefore, p-FRET with laser-based TIR illumination should present no insurmountable obstacles for calculation of the appropriate ($x$-$y$)-dependence of the $\boldsymbol{\alpha}$ matrix.

With the calculated concentrations for the three species, we chose to make normalized concentration images that display the fraction of total molecules that are free donor, free acceptor, or FRET pair. However, there are many others ways the data can be displayed once the nonnormalized concentration have been calculated, e.g., concentration can be represented as a fraction of donor in complex, a fraction of acceptor in complex, and total donor to total acceptor (such as presented in Hoppe et al., 2002).

P-FRET might be uniquely useful in cell biological applications to record transient events that lead to FRET, for example, the interaction of secretory granules with the plasma membrane just before and during exocytosis. In such situations, speed and simultaneous viewing of both donor and acceptor is important, and quantitative spectroscopic aspects of FRET (such as the transfer efficiency in FRET complexes) are not as important. We estimate, based on typical sample brightness, improvements (as mentioned) in detection, and the noise predictions shown in Fig. 6 *A*, that statistical accuracies of $\pm 0.2$ in $\hat{C}_3$ should be attainable with subsecond exposure times.

The authors thank Dr. Joel Swanson for his interest and for providing the transfected cells, and Dr. Ronald Holz for his encouragement, support, and comments. We thank Nikon USA Inc. for providing microscopy equipment through their Partners in Research Program.

This project was supported by National Institutes of Health grant NS38129 (to D.A.), a National Institutes of Health Molecular Biophysics Training Grant Fellowship (to A.M.), a Guidant Award Fellowship (to A.M.), a Michigan Economic Development Corporation and the Michigan Life Sciences Corridor Grant (to Dr. Ronald W. Holz (University of Michigan)).

## REFERENCES


Axelrod, D. 1979. Carbocyanine dye orientation in red cell membrane studied by microscopic fluorescence polarization. *Biophys. J.* 26:557–574.

Berney, C., and G. Danuser. 2003. FRET or no FRET: a quantitative comparison. *Biophys. J.* 84:3992–4010.

Erickson, M. G., B. A. Alseikhan, B. Z. Peterson, and D. T. Yue. 2001. Preassociation of calmodulin with voltage-gated Ca(2+) channels revealed by FRET in single living cells. *Neuron.* 31:973–985.

Gautier, I., M. Tramier, C. Durieux, J. Coppey, R. B. Pansu, J.-C. Nicolas, K. Kemnitz, and M. Coppey-Moisan. 2001. Homo-FRET microscopy in living cells to measure monomer-dimer transition of GFP-tagged proteins. *Biophys. J.* 80:3000–3008.

Gordon, G. W., G. Berry, X. H. Liang, B. Levine, and B. Herman. 1998. Quantitative fluorescence resonance energy transfer measurements using fluorescence microscopy. *Biophys. J.* 74:2702–2713.

Griesbeck, O., G. S. Baird, R. E. Campbell, D. A. Zacharias, and R. Y. Tsien. 2001. Reducing the environmental sensitivity of yellow fluorescent protein: mechanism and applications. *J. Biol. Chem.* 276:29188–29194.

Habuchi, S., M. Cotlet, J. Hofkens, G. Dirix, J. Michiels, J. Vanderleyden, V. Subramaniam, and F. C. De Schryver. 2002. Resonance energy transfer in a calcium concentration-dependent cameleon protein. *Biophys. J.* 83:3499–3506.

Hoppe, A., K. Christensen, and J. A. Swanson. 2002. Fluorescence resonance energy transfer-based stoichiometry in living cells. *Biophys. J.* 83:3652–3664.

Janetopoulos, C., T. Jin, and P. Devreotes. 2001. Receptor-mediated activation of heterotrimeric G-proteins in living cells. *Science.* 291:2408–2411.

Kraynov, V. S., C. Chamberlain, G. M. Bokoch, M. A. Schwartz, S. Slabaugh, and K. M. Hahn. 2000. Localized Rac activation dynamics visualized in living cells. *Science.* 290:333–337.

Lakowicz, J. R. 1999. Principles of Fluorescence Spectroscopy. Kluwer Academic/Plenum, New York, NY.

Oliveria, S. F., L. L. Gomez, and M. L. Dell'Acqua. 2003. Imaging kinase-AKAP79-phosphatase scaffold complexes at the plasma membrane in living cells using FRET microscopy. *J. Cell Biol.* 160:101–112

Varma, R., and S. Mayor. 1998. GPI-anchored proteins are organized in submicron domains at the cell surface. *Nature.* 394:798–801.

Xia, Z., and Y. Liu. 2001. Reliable and global measurement of fluorescence resonance energy transfer using fluorescence microscopes. *Biophys. J.* 81:2395–2402.